

Control of transition metal - oxygen bond strength boosts the redox ex- solution in perovskite oxide surface

Kyeounghak Kim^{a,‡}, Bonjae Koo^{b,‡}, Yong-Ryun Jo^c, Siwon Lee^b, Jun Kyu Kim^b, Bong-Joong
Kim^{c,*}, WooChul Jung^{b,*}, and Jeong Woo Han^{a,*}

^aDepartment of Chemical Engineering, Pohang University Science and Technology (POSTECH), Pohang, Gyeongbuk 37673, Republic of Korea

^bDepartment of Materials Science and Engineering, Korea Advanced Institute of Science and Technology (KAIST), Daejeon 34141, Republic of Korea

^cSchool of Materials Science and Engineering, Gwangju Institute of Science and Technology (GIST), Gwangju 61005, Republic of Korea

Supplementary information

*Corresponding authors: jwhan@postech.ac.kr, wjung@kaist.ac.kr, kimbj@gist.ac.kr

[‡]K. K. and B. K. contributed equally to this work.

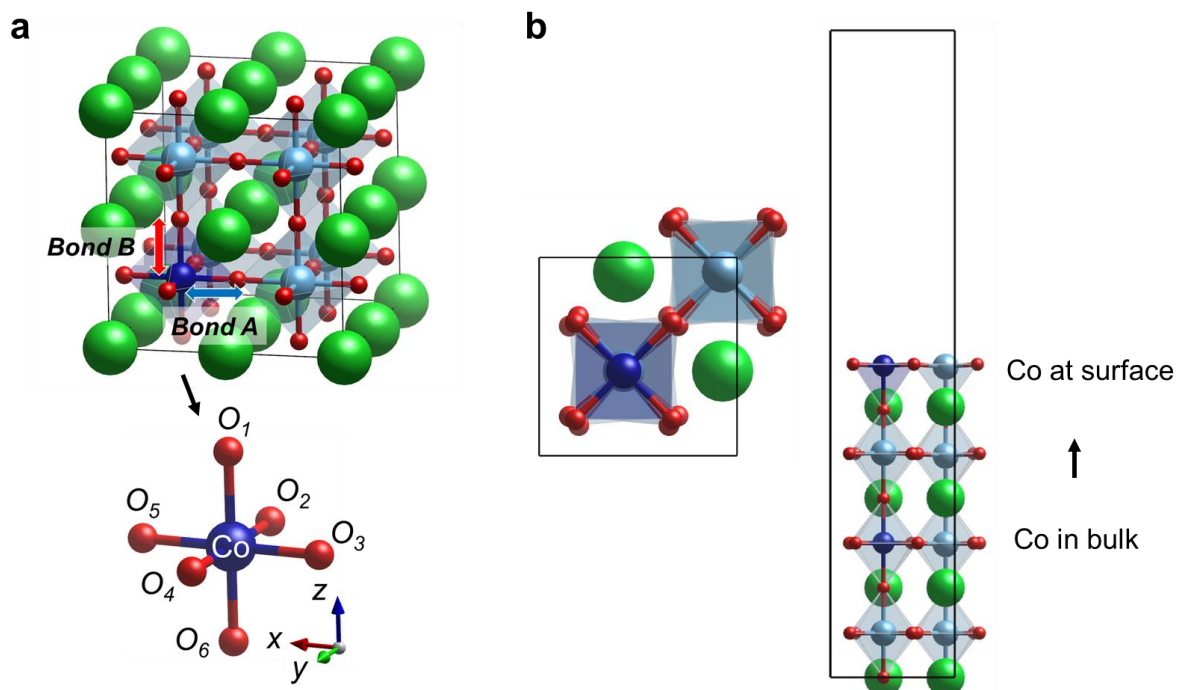


Fig. S1 (a) Bulk and (b) slab model of $\text{SrTi}_{0.75}\text{Co}_{0.25}\text{O}_3$ (STC). Sr, Ti, Co, and O atoms are colored by green, sky blue, blue and red, respectively. The O_1 to O_6 are oxygen positions bounded to Co in bulk.

In the computational aspects, we also measured two types of Co-O bonds because Co cation binds with surrounding oxygen atoms *via* four in-plane (x - y plane) bonds and two out-of-plane (z direction) bond under different biaxial strain states, which responded differently to the applied strain to maintain the Poisson ratio of the crystal structure (Fig. S1a). Therefore, the in-plane and out-of-plane bond lengths are increased and decreased, respectively as more tensile strain applied. However, the average length of Co-O bonds ultimately increased under biaxial strain states (Table S1). On the other hand, under isostatic tensile (compressive) strain, the bond lengths of the in-plane Co-O bonds and the out-of-plane Co-O bonds are simultaneously increased (decreased) with a same ratio regardless of the direction (x -, y -, or z -).

Unfortunately, the detailed atomic-level mechanism of the ex-solution process has not been revealed till now, and much debate remains about it in the relevant academic community. In our experiments, the composition in bulk perovskite materials was not significantly changed after ex-solution, while dopant elements (Co in this study) were enriched at surface. Therefore, we can reasonably think that Co atoms segregated toward the surface by the sequential exchange processes of bulk Co to nearest-neighbored host cation. The thermodynamic driving force of Co segregation was expressed as the Co segregation energy, which was calculated by total energy difference between Co located in bulk and at surface. Since the energy is a state function, it can be interpreted regardless of detailed paths.

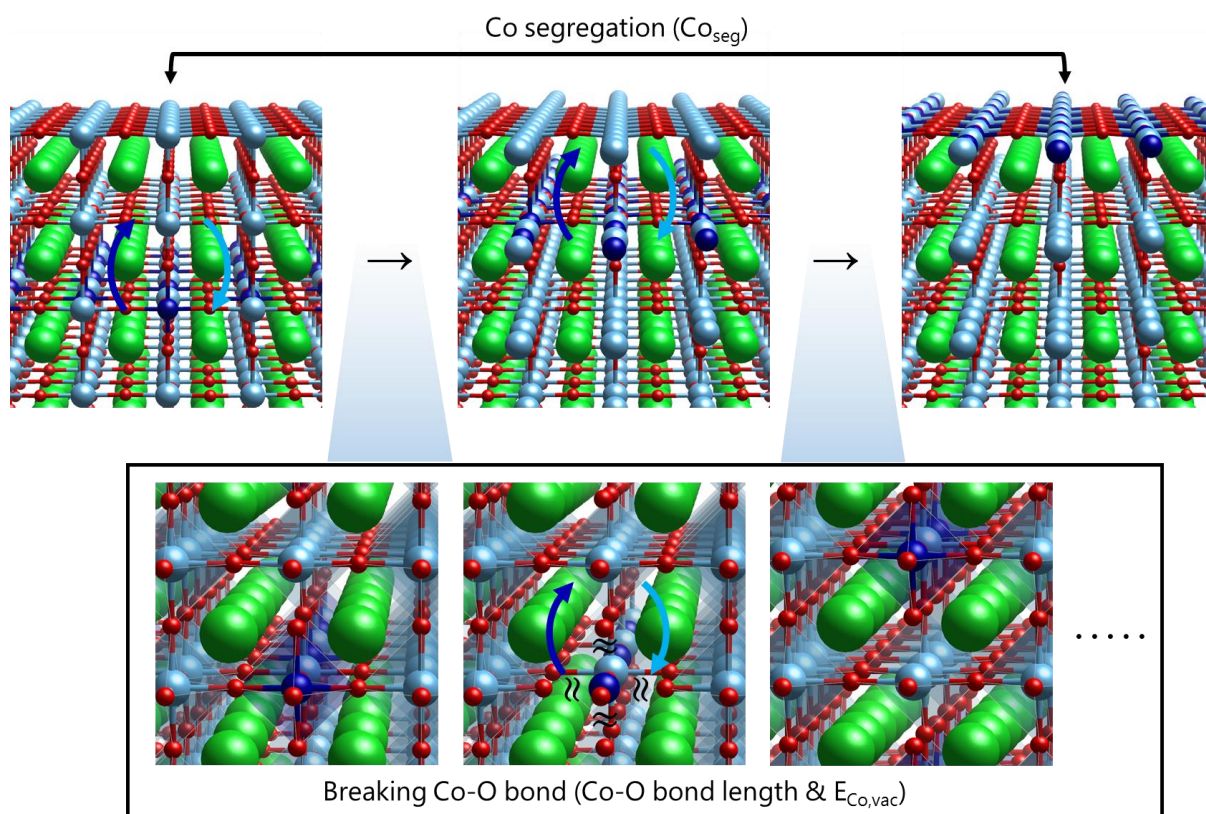


Fig. S2 Schematic illustration of Co ex-solution mechanism and its fundamental driving force.

Table S1 The bond length [\AA] of Co-O in STC under biaxial strain states. The O₁ to O₆ are oxygen atoms corresponding to Fig. S1a.

	-3.0	-2.5	-2.0	-1.5	-1.0	-0.5	0.0	+0.5	+1.0	+1.5	+2.0	+2.5	+3.0
O ₁ -Co	1.9537	1.9500	1.9467	1.9434	1.9398	1.9365	1.9469	1.9309	1.9271	1.9240	1.9197	1.8777	1.8727
O ₂ -Co	1.8348	1.8437	1.8524	1.8618	1.8707	1.8797	1.8892	1.8932	1.9075	1.9156	1.9263	1.9767	1.9528
O ₃ -Co	1.8348	1.8437	1.8524	1.8618	1.8707	1.8797	1.8892	1.8932	1.9075	1.9156	1.9263	1.9403	1.9871
O ₄ -Co	1.8348	1.8437	1.8524	1.8618	1.8707	1.8797	1.8892	1.8932	1.9075	1.9156	1.9263	1.9767	1.9528
O ₅ -Co	1.8348	1.8437	1.8524	1.8618	1.8707	1.8797	1.8892	1.8932	1.9075	1.9156	1.9263	1.9403	1.9871
O ₆ -Co	1.9537	1.9500	1.9467	1.9434	1.9398	1.9365	1.9469	1.9309	1.9271	1.9240	1.9197	1.8777	1.8727
In-plane	1.8348	1.8437	1.8524	1.8618	1.8707	1.8797	1.8892	1.8932	1.9075	1.9156	1.9263	1.9585	1.9699
Out-of-plane	1.9537	1.9500	1.9467	1.9434	1.9398	1.9365	1.9469	1.9309	1.9271	1.9240	1.9197	1.8777	1.8727
Average	1.8744	1.8792	1.8838	1.8890	1.8937	1.8986	1.9085	1.9058	1.9140	1.9184	1.9241	1.9315	1.9375

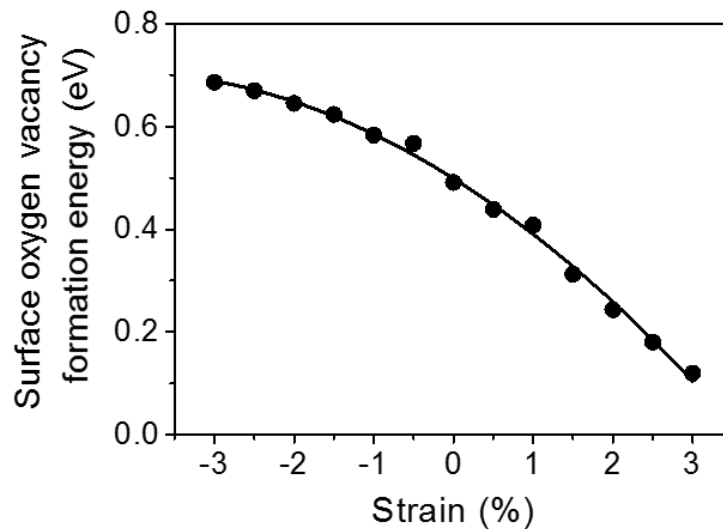


Fig. S3 DFT-calculated surface oxygen vacancy formation energy in STC slab model as a function of biaxial strain.

In our experiments, we fabricated strained epitaxial STC thin films and quantitatively analyzed their crystal structure via HR-XRD in both in-plane and out-of-plane directions. The (001)-direction epitaxial STF has two different types of Co-O bonds: four in-plane Co-O bonds and two out-of-plane Co-O bonds (Fig. S1a). The average Co-O bond length used in this study is the average of these six values, which are shown in Table S2. It was confirmed that the relative in-plane tensile strain increases the average length of Co-O bonds in STC crystal lattice.

Table S2 Calculated Co-O bond length [\AA] of $\text{SrTi}_{0.75}\text{Co}_{0.25}\text{O}_{3-\delta}$ (STC) thin films. The strained in-plane and out-of-plane lattice parameters and Co-O bond lengths of STC films were extracted by combining the interplanar distance of the (002) and (110) peaks from the HR-XRD data.

Substrate	In-plane Co-O bond length [\AA] (bond A)	Out-of-plane Co-O bond length [\AA] (bond B)	Average Co-O [\AA]
LaAlO_3 (3.790 \AA)	1.905	1.967	1.926
SrTiO_3 (3.905 \AA)	1.929	1.966	1.944
DyScO_3 (3.948 \AA)	1.961	1.956	1.959

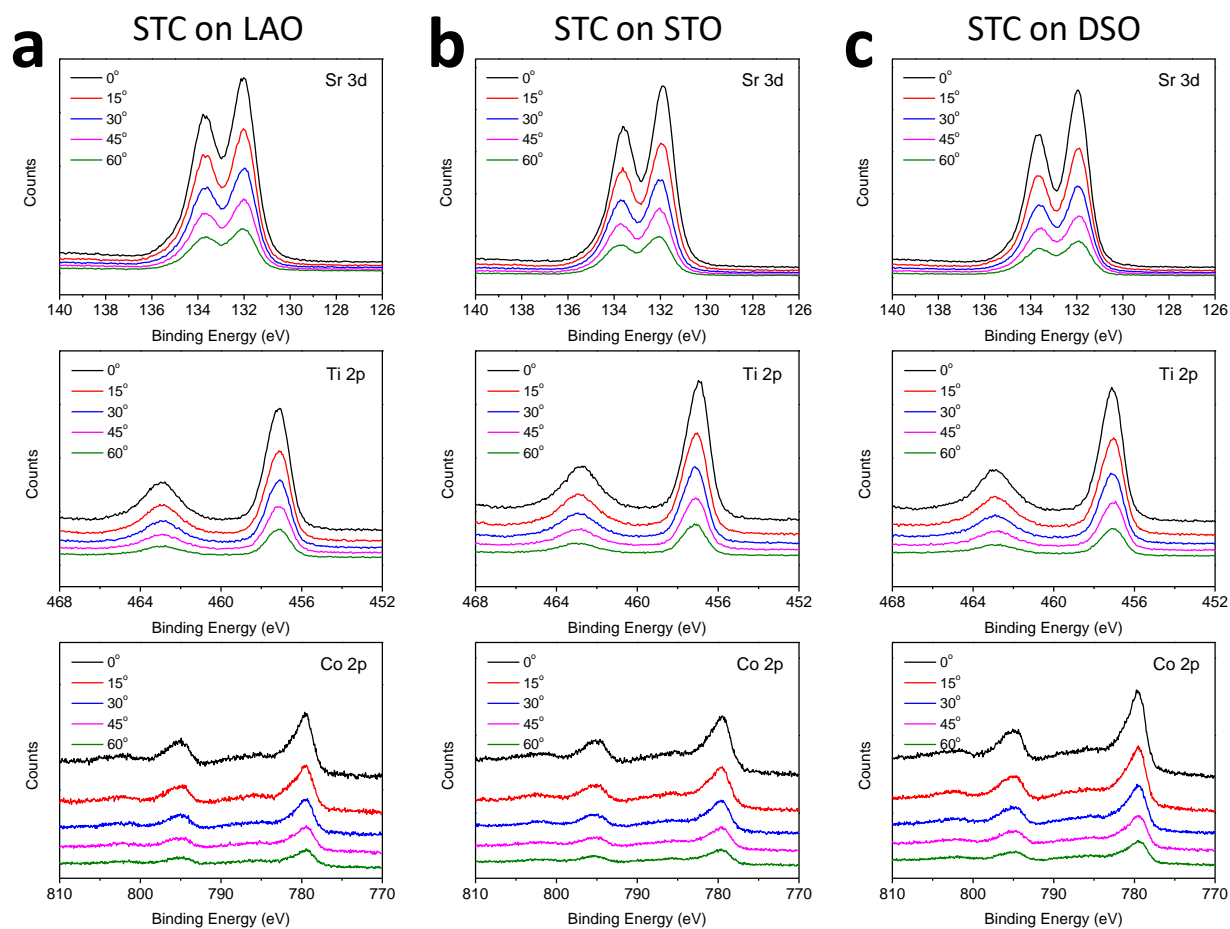


Fig. S4 (a) Sr 3d, Ti 2p and Co 2p spectra of epitaxial SrTi_{0.75}Co_{0.25}O_{3-δ} (STC) thin films on single-crystal LaAlO₃ (LAO), (b) SrTiO₃ (STO) and (c) DyScO₃ (DSO) substrates at emission angles of 0° to 60°.

Table S3 Comparison of the specific area from Sr 3d, Ti 2p and Co 2p AR-XPS spectra and the relative Co ratio from Fig. S3.

Substrate	Emission angle, θ (°)	Element	Area	At. %	Co/Sr	$I_{\theta^\circ}/I_{0^\circ}$
LaAlO ₃	0	Sr 3d	219627.4	45.7	0.29	1.00
		Ti 2p	144471.2	41.1		
		Co 2p	98422.6	13.2		
	15	Sr 3d	163604.7	45.2		
		Ti 2p	109918.4	41.6		
		Co 2p	74462.1	13.2		

SrTiO ₃	30	Sr 3d	120698.1	45.1	0.29	1.00
		Ti 2p	81482.4	41.7		
		Co 2p	54699.4	13.2		
	45	Sr 3d	84685.9	45.4	0.33	1.15
		Ti 2p	53983.4	39.6		
		Co 2p	43626.9	15.0		
	60	Sr 3d	52013.5	44.2	0.38	1.33
		Ti 2p	33391.1	38.9		
		Co 2p	30931.5	16.9		
DyScO ₃	0	Sr 3d	254384.7	45.6	0.32	1.00
		Ti 2p	162380.6	39.8		
		Co 2p	127019.8	14.6		
	15	Sr 3d	187714.2	44.2	0.37	1.15
		Ti 2p	122118.4	39.4		
		Co 2p	107813.6	16.4		
	30	Sr 3d	137325.6	43.7	0.37	1.15
		Ti 2p	92397.5	40.2		
		Co 2p	78629.4	16.1		
45	Sr 3d	96854.0	44.1	0.39	1.22	
	Ti 2p	61975.3	38.6			
	Co 2p	59101.7	17.3			
60	Sr 3d	60242.5	44.0	0.44	1.37	
	Ti 2p	36545.9	36.6			
	Co 2p	41202.7	19.4			
DyScO ₃	0	Sr 3d	237194.8	42.9	0.46	1.00
		Ti 2p	151122.3	37.4		
		Co 2p	169810.0	19.7		
	15	Sr 3d	174205.9	42.3	0.50	1.08
		Ti 2p	109809.8	36.6		
		Co 2p	134667.2	21.1		
	30	Sr 3d	126354.4	40.7	0.56	1.22
		Ti 2p	82912.4	36.5		
		Co 2p	110136.7	22.8		
45	Sr 3d	86904.4	40.1	0.60	1.32	
	Ti 2p	56369.2	35.6			
	Co 2p	81898.2	24.3			
60	Sr 3d	52898.9	39.5	0.68	1.50	
	Ti 2p	32440.3	33.2			
	Co 2p	56690.9	27.3			

Fig. S5 a-c shows Co 2p spectra of epitaxial STC films on single-crystal LaAlO₃ (LAO), SrTiO₃ (STO) and DyScO₃ (DSO) substrates at emission angles of 0° and 60°. The Co 2p spectra can be deconvoluted into three double-let peaks taking account of Co oxidation state. The relative Co²⁺ ratio increased continuously with increasing lattice strain (Fig. S5d). In-plane stretched film on DSO shows significantly greater Co²⁺-excess at the surface compared to the compressed STC films.

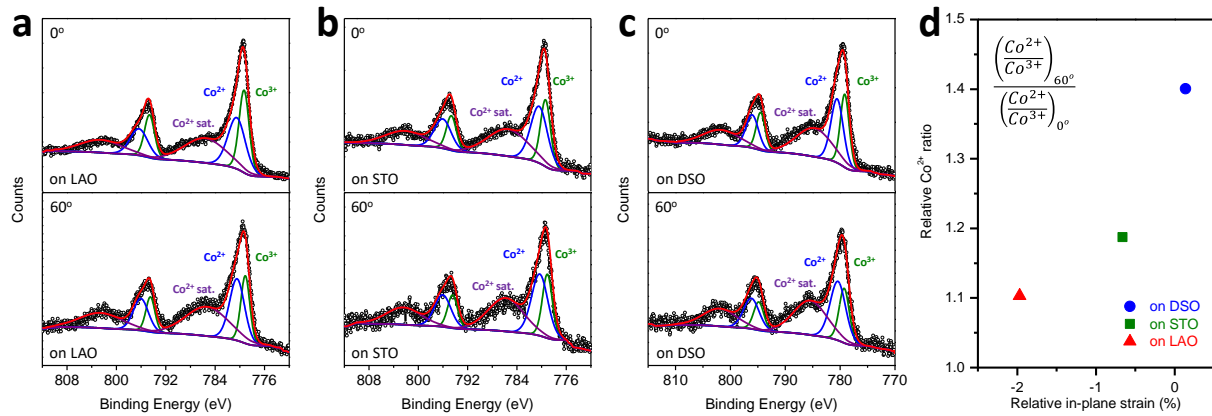


Fig. S5 (a) Co 2p spectra of epitaxial SrTi_{0.75}Co_{0.25}O_{3-δ} (STC) thin films on single-crystal LaAlO₃ (LAO), (b) SrTiO₃ (STO) and (c) DyScO₃ (DSO) substrates at emission angles of 0° and 60°. (d) The relative Co²⁺ ratio of epitaxial STC thin films with the degree of induced in-plane strain.

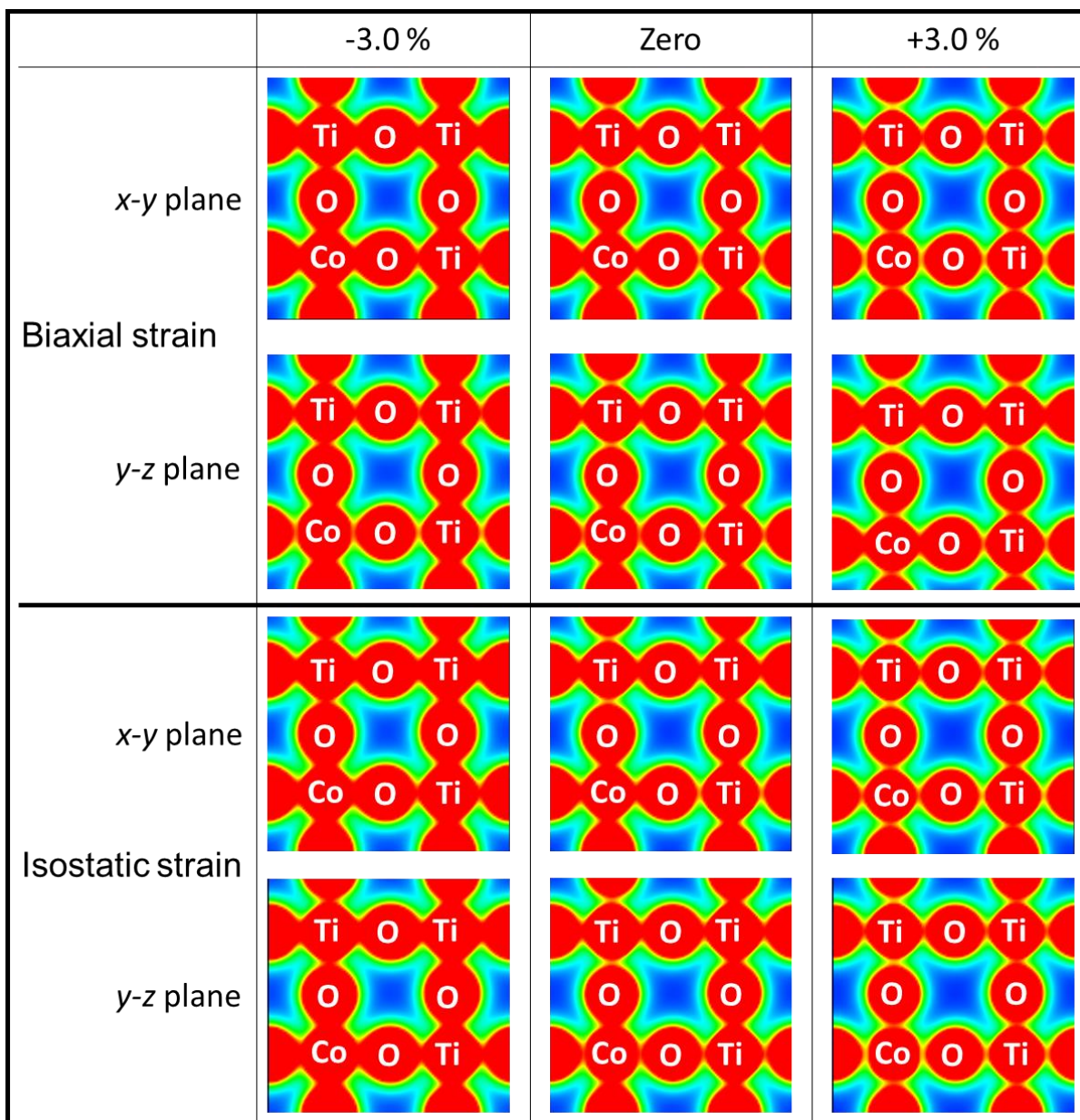


Fig. S6 Charge density distribution of *x-y* and *y-z* planes in SrTi_{0.75}Co_{0.25}O₃ (STC) under biaxial and isostatic strain, respectively.

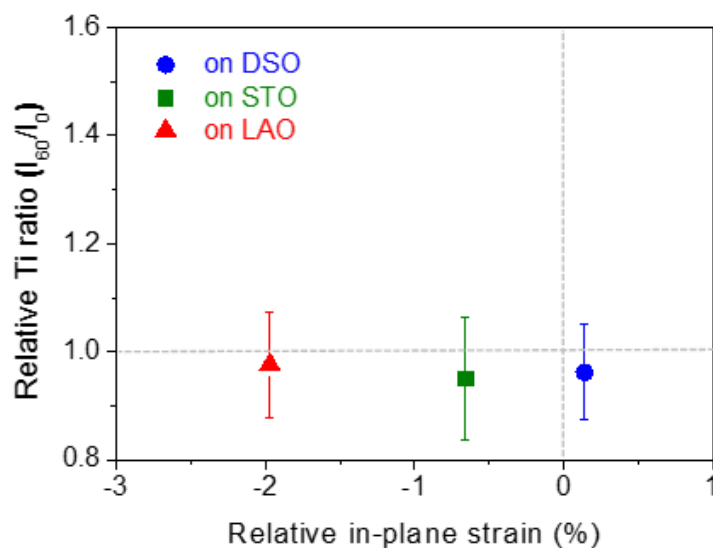


Fig. S7 Relative Ti ratio of epitaxial $\text{SrTi}_{0.75}\text{Co}_{0.25}\text{O}_{3-\delta}$ (STC) thin films on single-crystal LaAlO_3 (LAO), SrTiO_3 (STO) and DyScO_3 (DSO) substrates measured by AR-XPS according to degree of induced in-plane strain.

To determine the strain state of Co in BSTC compared with that in STC, we measured Co-O bond lengths in a same way as isostatic strain states because the size effect from the ionic radius difference between dopant Ba and host Sr affects the change in bond length of Co-O and Ti-O equally in all x -, y -, and z -directions. However, the degree of applied strain is not the same as the isostatic strain because of several reasons; (1) dopant mainly induces local strain to surrounding oxygen atoms, (2) dopant distribution also affects the change in bond length of Co-O, and (3) cell volume is also changed by the Ba from 481.98 \AA^3 (STC) to $490.28 \sim 490.63 \text{ \AA}^3$ (BSTC). We constructed several possible configuration of Ba dopants in BSTC as shown in Fig. S8. The bond lengths of Co-O are increased in all x -, y -, and z -directions as are under isostatic strain except for CON1. However, regardless of dopant configurations, the average bond lengths of Co-O and the cell volumes are increased together. Therefore, we believe that isostatic strain curves can be effectively applied for predicting the stability of B-site cation under aliovalent doping of A-site cation in the perovskite materials.

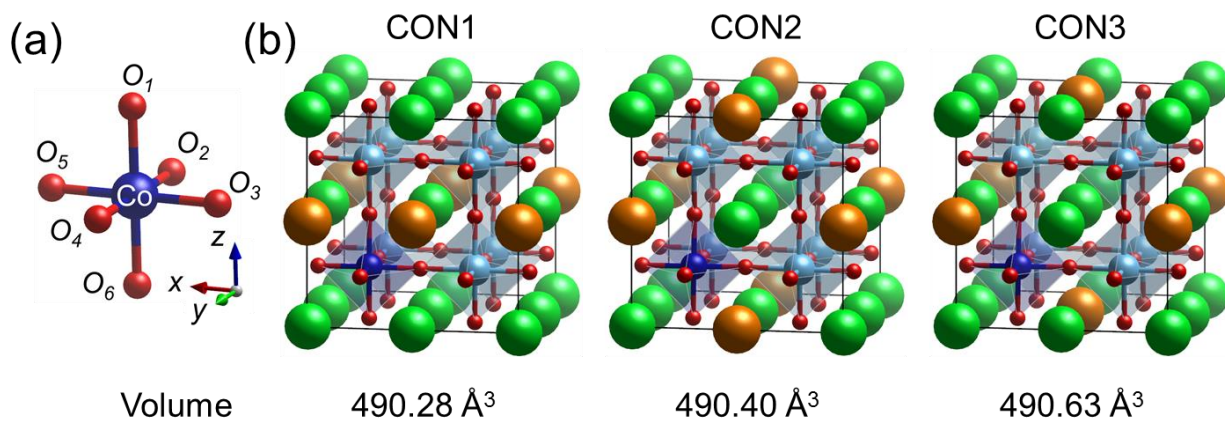
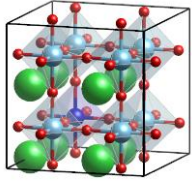
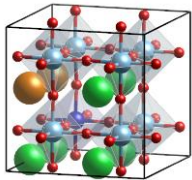


Fig. S8 (a) The oxygen positions (O_1 to O_6) bonded to Co in (b) three possible Ba configurations of bulk $Ba_{0.25}Sr_{0.75}(Ti_{0.75}Co_{0.25})O_3$ (BSTC). Ba, Sr, Ti, Co, and O atoms are colored by orange, green, sky blue, blue and red, respectively.

Table S4 The bond length [\AA] of Co-O in BSTC and STC under a strain free state. The O_1 to O_6 are the oxygen atoms corresponding to Fig. S8.

Co- O_x [\AA]	CON1	CON2	CON3	STC
O_1	1.9522	1.9300	1.9242	1.9469
O_2	1.9040	1.8942	1.9169	1.8892
O_3	1.9049	1.9246	1.9165	1.8892
O_4	1.9435	1.9115	1.9169	1.8892
O_5	1.9049	1.9246	1.9165	1.8892
O_6	1.9080	1.9300	1.9242	1.9469
In-plane	1.9261	1.9151	1.9186	1.9036
Out-of-plane	1.9064	1.9273	1.9204	1.9181
Average	1.9196	1.9192	1.9192	1.9084

Table S5 DFT-calculated Co-O bond length, Co vacancy formation energy, and optimized structure of bulk $\text{SrTi}_{0.75}\text{Co}_{0.25}\text{O}_3$ (STC) and $\text{Ba}_{0.25}\text{Sr}_{0.75}\text{Co}_{0.25}\text{O}_3$ (BSTC).

	Co-O Bond length [\AA]	Co vacancy formation energy [eV]	Structure
STC	1.906	4.93	
BSTC	1.920	4.73	

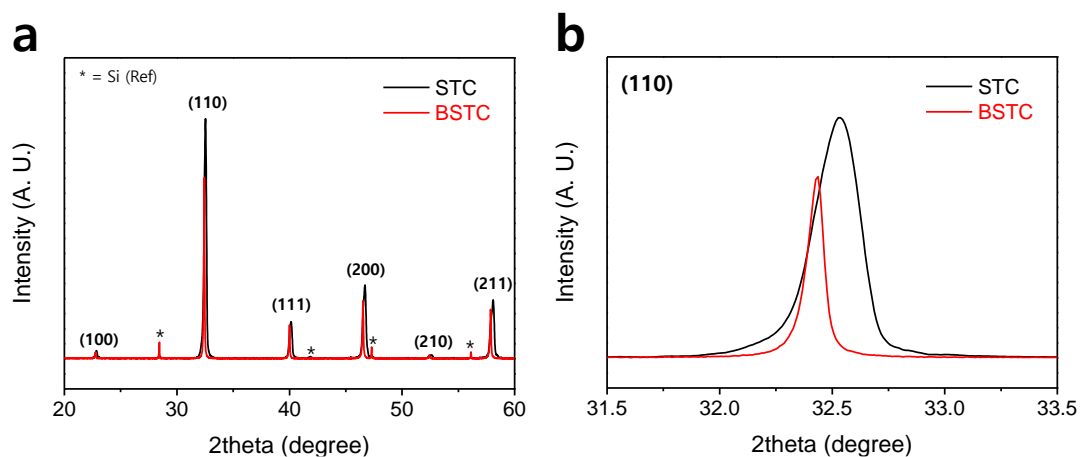


Fig. S9 (a) High-resolution powder X-ray diffraction (HR-powder XRD) result of $\text{SrTi}_{0.75}\text{Co}_{0.25}\text{O}_{3-\delta}$ (STC) with or without 5 at.% Ba doping. (b) The detail patterns in (110) plane of STC powder with or without 5 at.% Ba doping.

Table S6 Calculated lattice parameter and Co-O bond length [\AA] of $\text{SrTi}_{0.75}\text{Co}_{0.25}\text{O}_{3-\delta}$ (STC) with or without 5 at.% Ba doping from the HR-XRD data in Fig. S9.

Material	Lattice parameter [\AA]	Average Co-O [\AA]
STC	3.889	1.944
BSTC	3.901	1.951

Table S7 Molar fraction of a polycrystalline $\text{SrTi}_{0.75}\text{Co}_{0.25}\text{O}_{3-\delta}$ (STC) thin film with or without 5 at.% Ba doping measured by X-ray fluorescence (XRF) analysis.

Material	Ba	Sr	Ti	Co
STC		100.74	75.00 (Ref.)	24.40
BSTC	3.60	95.00	75.00 (Ref.)	24.43

For the distribution of metal particles synthesized by ex-solution, we carried out an SEM analysis of the $\text{SrTi}_{0.75}\text{Co}_{0.25}\text{O}_{3-\delta}$ (STC) polycrystalline thin films with/without Ba dopant after CO oxidation measurements (Fig. 4e and f). It is clear that ex-solved Co nanoparticles were uniformly synthesized and well-dispersed on the surface of STC and Ba-doped STC films. The size (diameter) distribution of two samples is quite similar to each other, with an average particle size of 23.6 ± 4.1 nm (STC) and 21.8 ± 5.3 nm (BSTC), respectively. However, the number density of particles is more observed in the BSTC film (i.e., $179.9 /\mu\text{m}^2$ (STC) vs. $265.1 /\mu\text{m}^2$ (BSTC)).

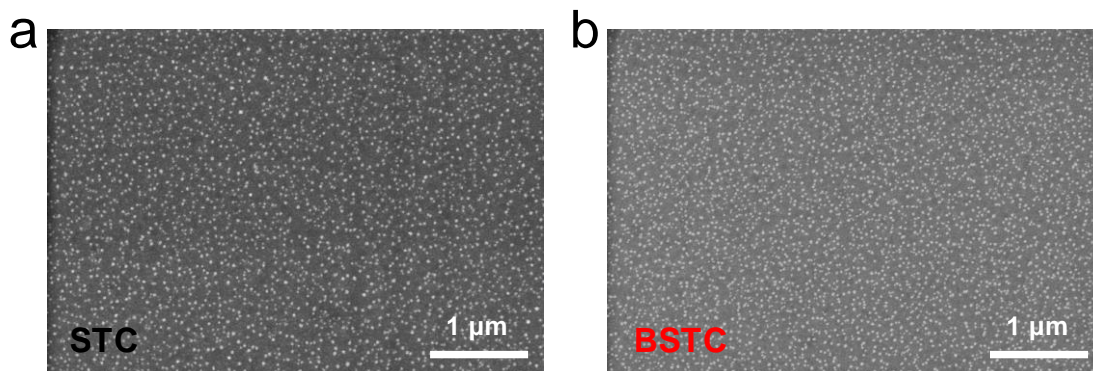


Fig. S10 (a) Surface morphology of polycrystalline SrTi_{0.75}Co_{0.25}O_{3-δ} (STC) thin films after catalytic activity test of CO oxidation by scanning electron microscopy (SEM) techniques and (b) with 5 at.% Ba doping.

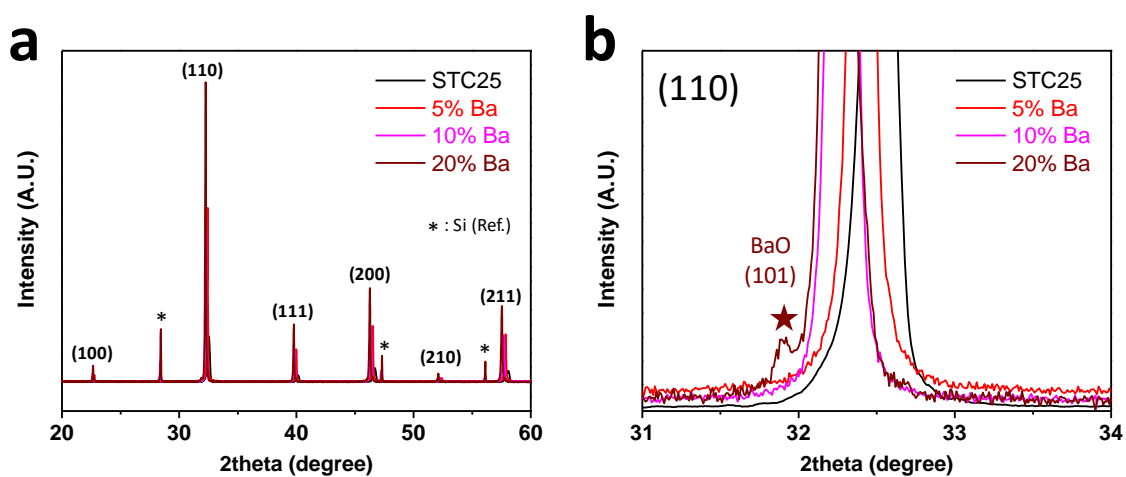


Fig. S11 (a) High-resolution powder X-ray diffraction (HR-powder XRD) result of SrTi_{0.75}Co_{0.25}O_{3-δ} (STC) with 5, 10, and 20 at.% Ba doping. (b) The detail patterns in (110) plane of STC powder with 5, 10 and 20 at.% Ba doping.

Table S8 Calculated lattice parameter and Co-O bond length [\AA] of $\text{SrTi}_{0.75}\text{Co}_{0.25}\text{O}_{3-\delta}$ (STC) with 5, 10, 20 at.% Ba doping from the HR-XRD data in Fig. S11. (Note: 20 at% Ba doping caused a Ba-rich secondary phase, which is due to the relatively low solubility of Ba in STC.)

Material	Lattice parameter [\AA]	Average Co-O [\AA]
STC	3.889	1.945
with 5% Ba	3.901	1.951
with 10% Ba	3.907	1.954
with 20% Ba	3.920	1.960

To clearly confirm the effect of Ba doping in STC, we quantified the size (diameter), number density, and perimeter length of ex-solved Co nanoparticles via SEM image analysis and compared the results (Table S9). Co particles of similar size, whether Ba doped or not, are uniformly produced on the STC surface, but more particles are observed in the Ba-doped sample. These observations evidently support that Ba doping can promote Co ex-solution.

Table S9 Quantitative analyses of ex-solved Co nanoparticles on the surfaces of $\text{SrTi}_{0.75}\text{Co}_{0.25}\text{O}_{3-\delta}$ (STC) thin films after catalytic activity test of CO oxidation with 5 at.% Ba doping. The data were collected from the SEM image as shown in Fig. 4e, f, and S10.

	Diameter (nm)	Density ($\#/\mu\text{m}^2$)	Perimeter (nm)	Total surface area (nm^2)	Total volume (nm^3)
STC	23.6 ± 4.1	179.9	7186.3	87375.4	364125.5
BSTC	21.8 ± 5.3	265.1	9790.7	112983.8	455931.6

Turnover frequency (TOF) values normalized by a perimeter of ex-solved Co atoms could be identified as the dominant active site for CO oxidation are very similar to the reported result in *J. Am. Chem. Soc.*, 2019, **141**, 6690–6697.

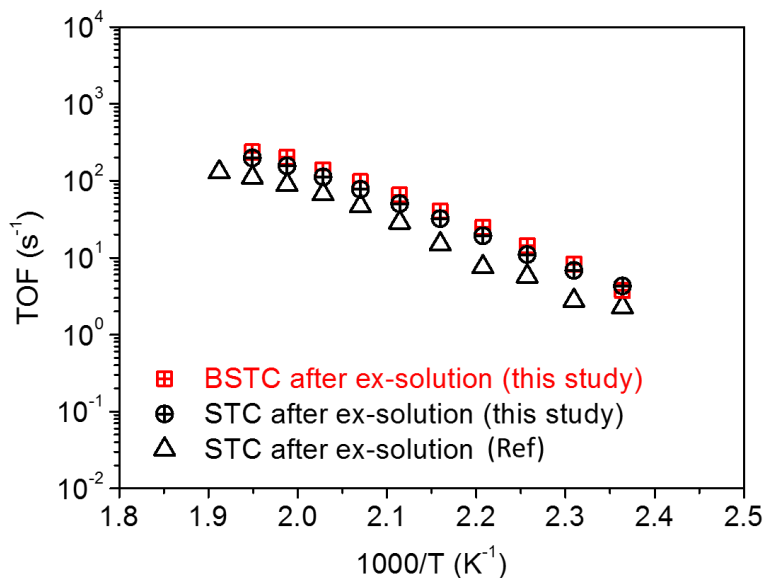


Fig. S12 Turnover frequencies (TOFs) for CO oxidation of polycrystalline STC thin film with or without 5 at.% Ba doping. Ref: *J. Am. Chem. Soc.*, 2019, **141**, 6690–669.

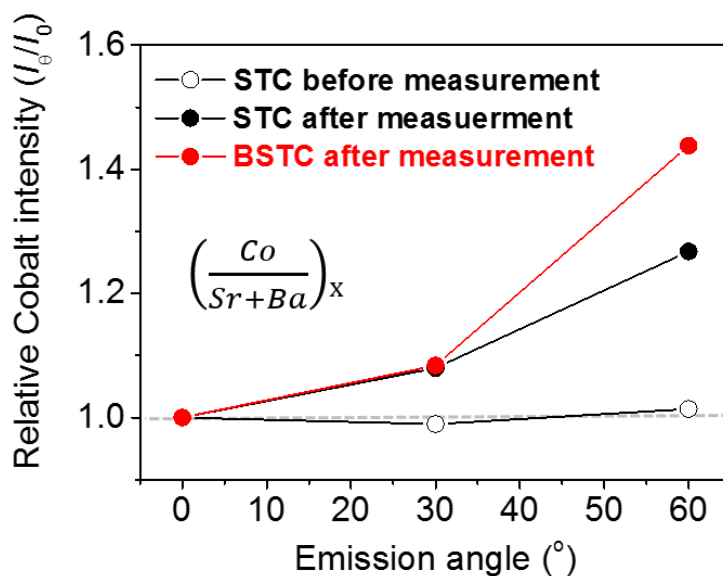


Fig. S13 Chemical composition change of polycrystalline $\text{SrTi}_{0.75}\text{Co}_{0.25}\text{O}_{3-\delta}$ (STC) thin films with or without 5 at.% Ba doping before/after catalytic activity test of CO oxidation by angle-resolved X-ray photoelectron spectroscopy (AR-XPS) techniques.